26

Surface Acoustic Wave Devices for Harsh Environment

Cinzia Caliendo
Istituto dei Sistemi Complessi, ISC-CNR, Area della Ricerca Roma 2, Rome Italy

1. Introduction

There is an increasing demand of electronic components for aerospace, aircraft industries, sensors, automotive, chemical and material processing applications, to name just a few, able to operate reliably and for long time at high-temperature. Measurements reliability requires the electronic components to be placed directly inside the extreme environment, and to withstand temperatures of several centigrade degrees with lifetimes of several hours. The device mounting and packaging, but first of all the device materials must be stable with the working temperature, otherwise temperature-induced stress may result in device's failures. Electroacoustic devices based on surface and bulk acoustic wave (SAW and BAW) technology must satisfy the requirements of low cost, high frequency, high-Q, low loss, large piezoelectric coupling and zero temperature coefficient of delay (TCD) to be key devices in the communication and sensor fields. The temperature stability of the piezoelectric crystal is an essential characteristic because of its direct link with the temperature sensitivity of the electroacoustic device operation frequency. The high operation frequency is an essential characteristic for SAW and BAW devices to be used in mobile phones, cordless headphones, alarm and security systems, military equipment, sensors, etc. The temperature stability and the high operation frequency demands can be met through a proper choice of the piezoelectric substrate crystal cut, new piezoelectric materials and/or multilayer configurations. The use of temperature stable cuts of single crystal bulk piezoelectric materials or temperature compensated multilayers represents two possible solutions to the temperature stability requirement. The use of high-resolution lithography techniques and/or of high SAW velocity materials is required in order to extend the upper limit of the electroacoustic device frequency range. Submicron feature sized interdigital transducers (IDTs) are required to implement GHz range SAW devices on *slow* piezoelectric materials, while micron feature sized IDTs can still be used on *fast* materials, since the SAW device centre frequency, $f = v/\lambda$, depends on both the phase velocity of the propagating medium, v, and on the acoustic wavelength λ, being the IDT's period $p = \lambda/2$. Conventional piezoelectric substrates, such as quartz, lithium niobate ($LiNbO_3$), and lithium tantalate ($LiTa0_3$) crystals, cannot be used above 500°C. Quartz ST cut is a temperature stable material but it shows an alpha-beta transition at 573°C, which causes the loss of piezoelectricity, and results in a non-operable device. SAW devices implemented on $LiNb0_3$ have been studied for a temporary usage at 400°C [1]; however the $LiNbO_3$ acoustic wave properties are highly dependent on temperature since it is a pyroelectric

material and has a TCD as high as ~75 ppm/°C. $LiTaO_3$ shows properties, such as a low Curie temperature (607°C), sensitivity to temperature variations (TCD = 22 ppm/°C for the X-112°Y cut) and a strong pyroelectricity, which limit its operation at elevated temperatures. Piezoelectric bulk single crystals such as $GaPO_4$, LGS ($La_5Ga_3SiO_{14}$) and its isomorphs (called LGX family group) substrates are widely investigated for the realization of SAW-based devices able to work at high temperature. LGS belongs to the trigonal class 32 group as quartz but it has no α-β transitions and can operate up to its melting temperature of 1470°. It shows zero or very low TCD cuts with zero power flow angle and higher electromechanical coupling coefficient than that of quartz [2]. Langasite based SAW devices are not suitable for operation in the GHz range as a consequence of their low phase velocity and high acoustic losses (from 1 to 0.01 dB/wavelength [3]). $GaPO_4$ has twice the sensitivity of quartz and many its physical constants are stable up to about 900°C, but the accessible frequencies are limited to values of 1 GHz as a consequence of quite high acoustic losses.

The technology of thin piezoelectric films (such as AlN) offers the opportunity of combining the properties of the substrate with those of the film: thus a composite arrangement of fast materials with opposite sign *TCD*s and a proper design of the electroacoustic configuration enable achieving a thermally stable SAW device operating in the GHz range.

Aluminium nitride (AlN) is a piezoelectric material that shows interesting properties, such as excellent thermal conductivity (180W/mK), low coefficient of thermal expansion (CTE, 4.1×10^{-6} °C^{-1}), and good resistance to thermal shock and caustic chemicals [4], that make it useful as protective coating and guarantee the stability of the AlN-based devices when they are in contact with extreme environments. It is currently being investigated due to its promising potentialities for high-temperature, high-power, and high-frequency electronics. It has demonstrated to be an ideal candidate for packaging SiC-devices for high-temperature applications [5] thanks to its CTE that closely matches those of Si (3.5×10^{-6} °C^{-1}) and SiC (3.7×10^{-6} °C^{-1}), high electrical resistivity, high mechanical strength, and chemical inertness. Reactively sputtered AlN films have been used as an effective encapsulant for GaN [6] at an annealing temperature of 1100°C substituting the standard dielectric encapsulants, such as SiO_2 and Si_3N_4, that are not viable at so high temperatures. AlN maintains its piezoelectricity up to 1200°C in vacuum and shows very high BAW and SAW velocities (~6000 m/s and 11300 m/s for transversal and longitudinal BAWs propagating along the z direction, 5607 m/s for SAWs propagating in the *z* plane) that make it the ideal candidate for microwave electroacoustic devices implementation. Furthermore, AlN can be grown in thin film form onto non piezoelectric substrates by techniques as simple as the rf reactive sputtering. Both the structural properties of the substrate and the experimental sputtering parameters (such as the reactive gas flow rate, the partial pressure of reactive and inert gasses, the substrate temperature, the rf power, and the substrate-target distance) affect the morphological and structural properties of the sputtered thin films. The requirements for a suitable substrate include also a thermal coefficient-of-expansion compatible with that of the film, high-temperature stability, machinability, good adherence of the AlN film: among the available substrates, silicon, platinum and sapphire satisfy these requirements. Al_2O_3, substrates have a wide range of industrial applications as structural ceramic and optical materials. Al_2O_3 is extensively used as a high temperature, corrosion resistant refractory material due to its hardness, chemical durability, abrasive resistance, mechanical strength, and good electrical insulation. Al_2O_3 shows good thermal conductivity (24 W/mK), high SAW velocity (in the range 5555 to 5706 m/s in the c-plane), positive TCD (~70 ppm/°C) and a CTE that closely matches that of AlN. The AlN/Al_2O_3 –based multilayers can withstand temperatures up to

900°C, thus allowing the realization of high frequency, temperature compensated dispersive electroacoustic devices for high temperature applications. Electroacoustic devices implemented on Si substrates offer the opportunity to integrate the device with the surrounding electronic circuitry on the same chip. Moreover, the opposite TCD of Si (~30 ppm/°C) and AlN (~ -30 ppm/°C) allows the realisation of zero-temperature-coefficient acoustic devices at the proper film thickness to be used as sensors and actuators where low loss, low thermal drift, high sensitivity and high signal-to-noise ratio are demanded [7, 8]. Pt is the material of choice for metallic components that have to withstand oxidation, thank to its high temperature coefficient of resistance: Pt can be grown in thin film form and both the IDTs and ground electrodes can be easily defined by lift off technique.
In the present chapter the sustainability of Pt and AlN films on sapphire and Si substrates for high temperature applications is assessed.

2. AlN-based SAW devices

Bulk piezoelectric single crystals, such as LGS and $GaPO_4$, can be used for the implementation of non dispersive SAW devices, such as delay lines, filters and resonators, and the SAW propagation characteristics, such as phase velocity, electroacoustic coupling efficiency K^2 and TCD, depend on the crystal cut and SAW propagation direction, as well as on the geometry of the IDTs . The SAW propagation is excited by IDTs located at the free surface of the piezoelectric substrate and directly exposed to the surrounding environment, as shown in figure 1.

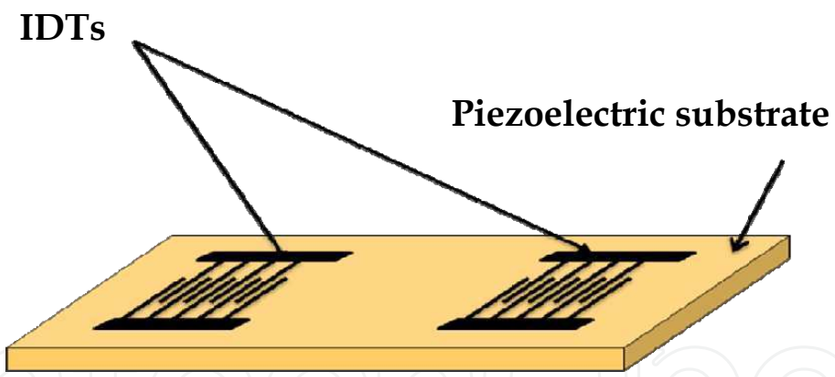

Fig. 1. SAW delay line on a piezoelectric substrate

AlN can be grown in thin film form onto non piezoelectric substrates, such as silicon or sapphire, thus allowing the realization of dispersive electroacoustic devices. Moreover, if the AlN film is sandwiched between the IDTs and the ground electrode, four piezoelectric coupling configurations can be obtained by placing the IDTs at the substrate/film interface or at the film surface, with and without the floating electrode opposite the IDTs. These four structures will be mentioned hereafter as substrate/film/IDT (SFT), substrate/IDT/film/metal (STFM), substrate/IDT/film (STF) and substrate/metal/film/IDT (SMFT), respectively. Figure 2a shows the top view of a dispersive SAW delay line, and figure 2b shows the cross sections of the four coupling configurations.
When the IDTs are located at the substrate/film interface, the piezoelectric film plays the role of both the acoustic wave transductor and protective layer of the underlying IDTs.

These four configurations show frequency dispersive SAW propagation characteristics, that are no longer solely determined by the geometry of the IDTs, the crystals cut, and the SAW propagation direction, but also by the film thickness and the electrical boundary conditions. For SAW propagating along layered structures, the achievable K^2 value is sometimes larger than that of the individual piezoelectric materials; it is frequency dispersive and depends on the type and orientation of the piezoelectric material, and it is drastically affected by the location of the IDTs and counter electrode with respect to the piezolectric layer. As an example, figures 3a and 3b show the K^2 vs film thickness to wavelength ratio, h/λ, for SAW propagation along *zx*- and *zy*-Al_2O_3/AlN for the four coupling configurations: the highest K^2 values obtainable are about 0.50 and 0.67% for STF x and y propagation (at $h/\lambda \sim 0.65$ and 0.60), 0.49 and 0.64 % for STFM x and y propagation (at $h/\lambda \sim 0.67$ and 0.62), being 0.3% the AlN K^2 value.

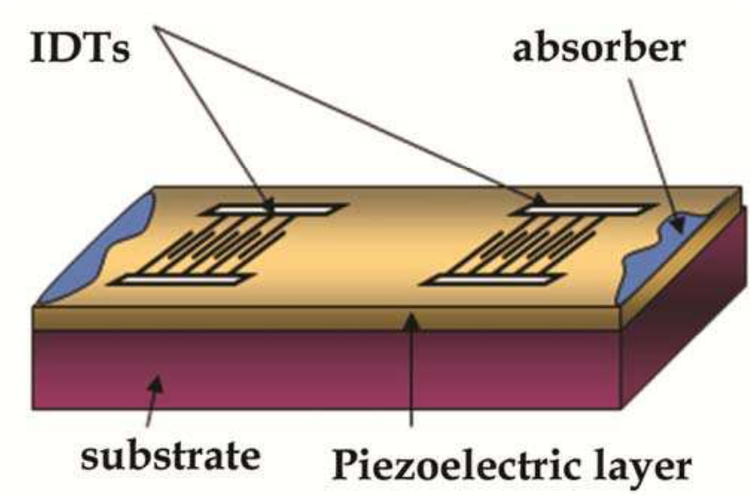

Fig. 2a. Dispersive SAW delay line

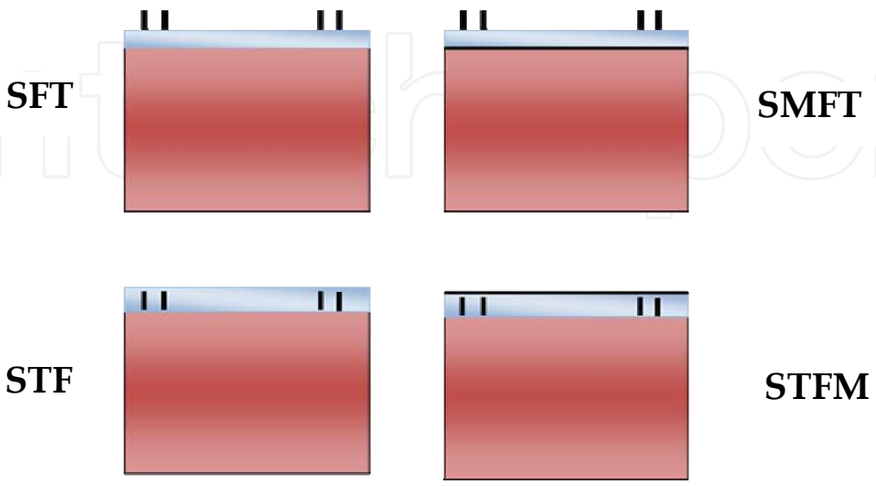

Fig. 2b. The four electroacoustic coupling configurations

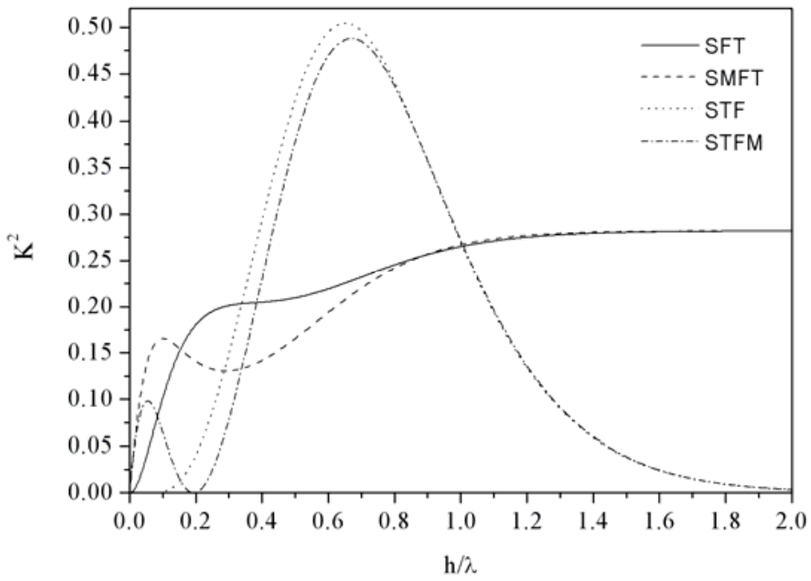

Fig. 3a. The K^2 vs h/λ for SAW propagating along zx-Al_2O_3/AlN for the four coupling configurations

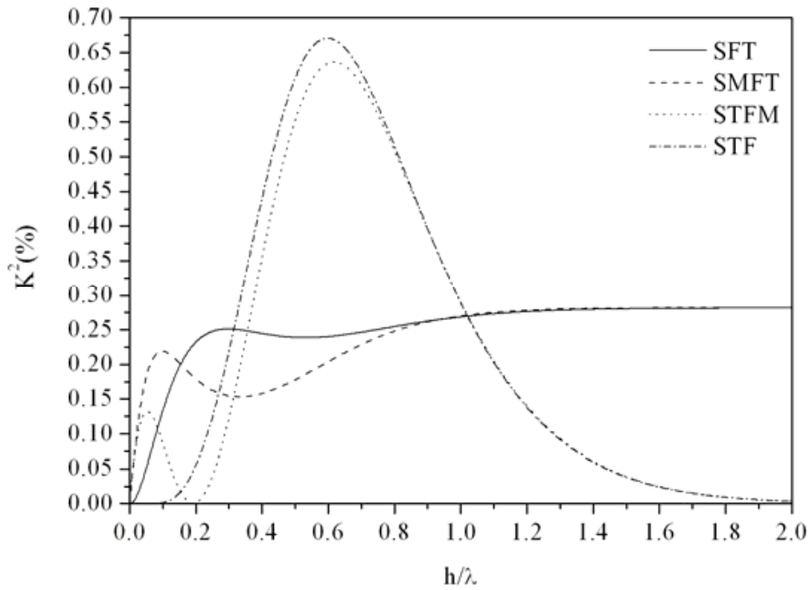

Fig. 3b. K^2 vs h/λ for SAW propagating along zy-Al_2O_3/AlN for the four coupling structures

Figures 4a and 4b show the K^2 vs h/λ for SAW propagation along Si/Pt/AlN and Si/AlN/Pt, being the Pt thickness the running parameter.

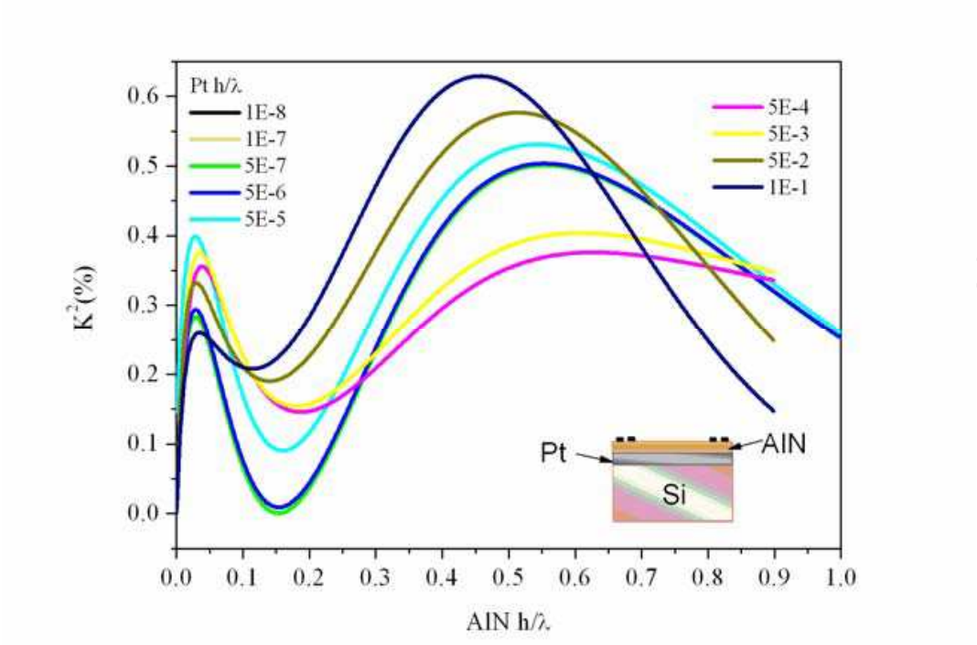

Fig. 4a. The K^2 vs AlN h/λ for SAW propagation along Si/Pt/AlN, for different Pt thickness values normalized to the acoustic wavelength

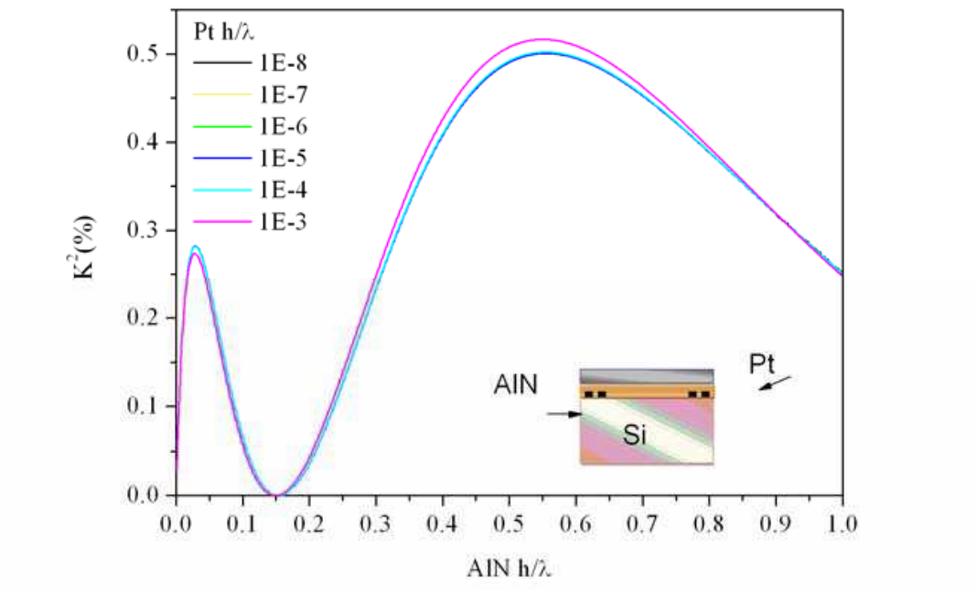

Fig. 4b. The K^2 vs AlN h/λ for SAW propagation along Si/AlN/Pt, for different Pt thickness values normalized to the acoustic wavelength

In figure 4a the highest K^2 values obtainable are in the range 0.5 to 0.63% at ~h/λ = 0.55 for Pt h/λ = 10^{-8} to 10^{-1}. In figure 4b the highest K^2 values obtainable are in the range 0.5 to

0.52% at ~h/λ = 0.555 for Pt h/λ = 10^{-8} to 10^{-3}. The theoretical data shown in figures 3 and 4 have been evaluated using the PC SAW software developed by Mc Gill University [9]. The theoretical K^2 has been approximated as $2\cdot\frac{v_{ph}^{f}-v_{ph}^{m}}{v_{ph}^{f}}$ where v_{ph}^{f} and v_{ph}^{m} are the SAW phase velocities along the free and electrically short-circuited surfaces of the AlN film. The phase velocity v_{ph}^{m} is obtained by the insertion of a perfectly conductive and infinitesimally thin film at the interfaces where the IDTs and the ground plane are located in each of the four coupling structure. The physical data relative to the elastic, piezoelectric and dielectric constants of AlN film are extracted from [10] and [11] and refer to single crystal AlN thin films grown on the basal plane of Al_2O_3(0001) by metalorganic vapor deposition. The *TCD* of the bulk piezoelectric crystal depends only on the crystal cut and the SAW propagation direction, while that of a layered structures is frequency dispersive. Because the SAW penetration depth inside the propagating medium is about one wavelength, in a layered medium, for $h/\lambda << 1$, the most of the SAW energy is confined to the substrate, while, as h increases with respect to λ, more and more of the SAW energy is confined to the film. For small AlN film thickness ($h/\lambda < 1$) the *TCD* value of the multilayer corresponds approximately to that of the substrate. With increasing the AlN film thickness respect to the acoustic wavelength ($h/\lambda \geq 1$) the *TCD* reaches the AlN *TCD* value. If the film and the substrate show opposite sign TCD values, there will be a h/λ value at which *TCD* = 0 ppm/°C (the temperature compensated point, TCP). This h/λ value represents the film thickness for which the two opposite sign *TCD*s of the film and of the substrate equilibrate to form a thermally compensated structure. Thus high-frequency, enhanced coupling, and thermally compensated elctroacoustic devices can be designed at the proper AlN films thickness values [12].

3. Materials and methods

Highly c-axis oriented AlN films were grown at 180°C and at 200°C by rf reactive sputtering technique on the polished surface of (0001) oriented single crystal Al_2O_3 substrate, on SiO_2/Si(100) and Pt/SiO_2/Si(100) substrates. The AlN deposition process parameters were the following: gas atmosphere of 100% of N_2, high purity (99.999%) 4" diameter Al target disc, RF power 200 watt, background vacuum $5\cdot10^{-8}$ Torr and pressure during the deposition process 3×10^{-3} Torr. Before starting the sputtering process, a 30 minute pre-sputtering was performed. The substrate temperature was held at 180 °C during the deposition process. The optimized sputtering parameters ensure AlN films showing a high adhesion to the substrate, c-axis orientation, a columnar growth, smooth surface, and high piezoelectricity; the films are also uniform, stress-free and extremely adhesive to the substrates. The Pt sputtering process parameters were the following: substrate temperature 200°C, gas atmosphere of 100% of Ar, high purity (99.99%) 4" diameter Pt target disc, RF power 150 watt, background vacuum 10^{-7} Torr and pressure during the deposition process 5×10^{-3} Torr. The deposition process of both Pt and AlN films is performed subsequently without breaking the vacuum in order to avoid any oxidation effects of the layers. Then the obtained samples were heated at 900°C in air at ambient pressure by a quartz tube furnace, for different lengths of time. The *cold* (20°C) sample was abruptly put inside the furnace pre-heated at 900°C and the annealing time was measured from the set temperature was reached; then the sample was removed from the furnace and brought abruptly to room

temperature. A temperature ramp of 1°C/s was measured by a thermocouple after the insertion of the *cold* sample inside the furnace. The furnace tube was not hermetically sealed, so ambient air was present during the loading and unloading of samples [14]. The structural properties of annealed Pt and AlN films were investigated by by X-ray diffraction measurements (XRD) a Seifert XRD 3003P performed on a a Seifert XRD 3003P diffractometer operating in the Bragg-Brentano geometry using Cu-Kα radiation (λ = 1.5418 Å) and the diffracted intensities were collected in θ-2θ scan mode in the range 20° <2θ < 80° with step size 0.04°. The reflection peaks of the diffractograms were compared with the standards of the JPCDS database. The crystallite size D was calculated from the Scherrer formula $D = \frac{0.9 \cdot \lambda}{B \cdot \cos \vartheta}$ where λ is the wavelength, B the θ-2θ full width at half maximum (FWHM) of the (0002) peak in rad and θ the Bragg angle. The *c* and *a* lattice parameters of the AlN and Pt films were calculated from the angular position of the AlN (002) and Pt (111) diffraction peaks of the θ-2θ scan and compared to the value from ref. 13 for Pt and powder AlN (*a* = 3.9231Å, *c* = 4.979Å). Since the electrical resistivity of the thin conducting films influences the device characteristics (such as insertion loss and Joule heating), the electrical resistance and the surface morphology of the outer Pt electrode were investigated at room temperature after each thermal annealing. The annealing effects on the piezoelectric constant d_{33} of the AlN films were also estimated [14].

3.1 Pt/AlN/Pt/SiO_2/Si

AlN films, 3.15 μm thick, were sputtered on bare and Pt (2200 Å thick) -covered SiO_2/Si(100) substrates, being ~2 μm the silicon oxide thickness; a Pt film (2200 Å thick) was sputtered on the AlN free surface and then the Pt/AlN/Pt/SiO_2/Si multilayers were heated at 900°C in air for lengths of time ranging from 1 to 32 hours. Figure 5 shows the XRD patterns of the as grown and annealed multilayers [14].

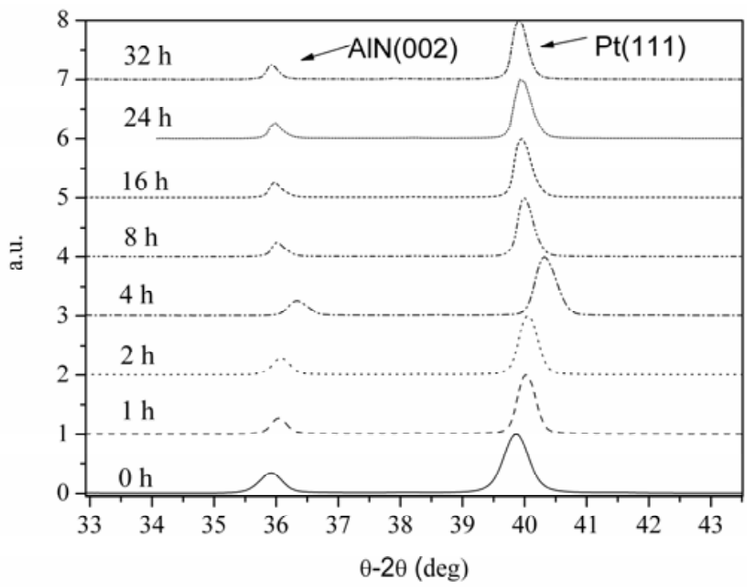

Fig. 5. XRD patterns of Pt/AlN/Pt/SiO_2/Si structures: the running parameter represents the annealing time

The piezoelectric AlN film is *c* axis oriented perpendicularly to the growth plane: in all the samples the AlN (002) and (004) peaks, at ~ 36° and at ~ 76°, are visible even after 32 hours annealing. The peak at 2ϑ ~40° corresponds to the Pt film strongly oriented along the (111) plane; with increasing the annealing time, a very small stress-induced shift in the Pt (111) peak position can be observed, while the same peak becomes narrower indicating a growing (111) fiber texture. As a consequence of the temperature-induced improvement of the Pt local epitaxy, the alignment precision of the AlN film crystalline planes also improves. The XRD data of the outer Pt film showed two peaks at 2θ~ 40° and 46.3° corresponding to the (111) and (200) orientations, and also a small platinum oxide (220) peak, at ~66°, clearly visible after the 1st annealing, that does not increase in percentage after the successive thermal cycles [14]. The AlN and Pt FWHM of the $\vartheta - 2\vartheta$ scan before and after the annealing [14] resulted improved, starting from 0.391 and 0.415° of the as grown AlN and Pt films, up to 0.24 and 0.28° after 32 hours annealing. The *c* and *a* lattice parameter of AlN and Pt films of the as-grown samples, calculated from the angular position of the (002) and (111) diffraction peaks, are respectively larger (4.997 Å) and smaller (3.914Å) than the values reported for bulk single crystal AlN and Pt [13], as a consequence of the lattice mismatch between the two materials. Figures 6 and 7 show the FWHM of the AlN(002) and Pt(111) peaks, and the *c* and *a* lattice parameters of AlN and Pt films vs the annealing time.

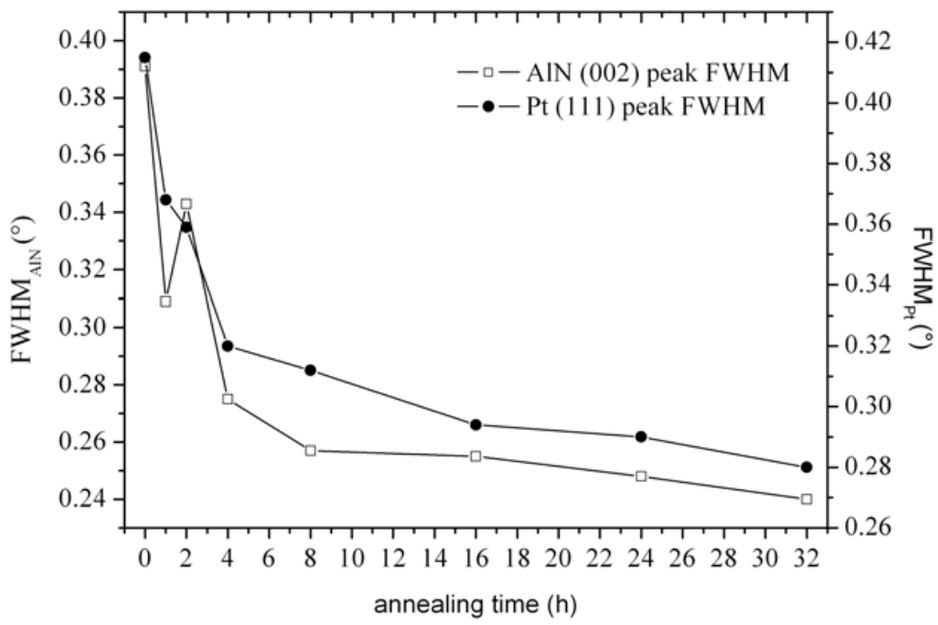

Fig. 6. FWHM of the AlN(002) and Pt(111) peaks vs annealing time

After the first annealings the AlN *c* parameter relaxes to the bulk while the Pt *a* parameter slightly decreases. Further annealings result in a permanent in-plane compressive stress for both the AlN and Pt films. The AlN(002) and Pt(111) peaks' FWHM decreases with increasing the annealing time indicating a decrease of inhomogeneous strain distribution.

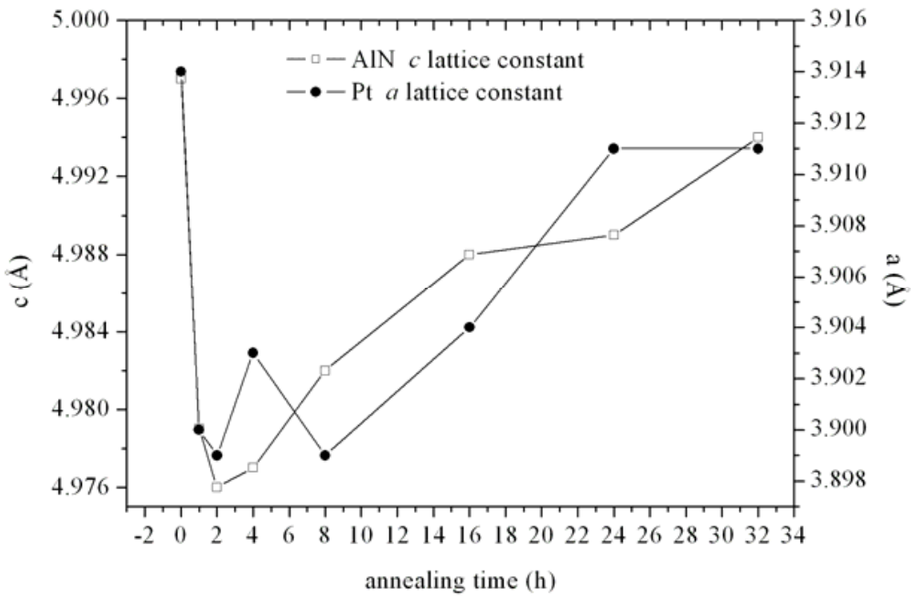

Fig. 7. *c* and *a* lattice parameters of AlN and Pt films vs the annealing time

The measurement of the longitudinal piezoelectric coefficient d_{33f} of the AlN film was done at ambient temperature on the same type multilayer without the outer Pt films, before and after the thermal annealing, with a method described in ref. 15 and based on the direct piezoelectric effect: a longitudinal acoustic wave perturbs the sample via a special probe and the electrical voltage induced in the piezoelectric film is measured. The probe consisted of a metal rod in contact with a $Pb(Zr,Ti)O_3$ (PZT)-based low frequency transducer that was connected to a pulse generator (pulse width 0.1-1.0 ns) to produce longitudinal bursts propagating along the metal rod. The contact between the rod and the piezoelectric film surface resulted in the application of a stress on the surface of AlN films. Stress-induced electrical charges were collected at the piezoelectric film surfaces by electrodes (the metal rod and the conducting substrate) and observed on a scope. The piezoelectric strain constant, d_{33f}, of the tested films was evaluated comparing the film response with the response of a thin single crystal reference sample, whose d_{33} was known. All the tested films showed to be piezoelectric with a difference in the d_{33f} obtained values not appreciable with this measurement technique because of an error of about 15-20 %. The estimated mean value is in the range from 6.2 and 7.4 pC/N, for both the as grown and all the annealed samples: these values well agree with the corresponding value reported in the available literature [16] that is about 6 pC/N.

The sheet resistivity of the Pt layer deposited on the $AlN/Pt/SiO_2/Si$ multilayer free surface was measured at ambient temperature by the four point method, before and after the thermal annealing. It was observed that the sheet resistance values decreases with increasing the annealing time, starting from ~0.6 Ω/sq, refereed to the unannealed samples, to ~0.5 Ω/sq, referred to the 32 hours annealed samples [14]. Scanning electron microscopy (SEM) investigations revealed an average grain size increased with increasing the annealing lasting. The as deposited Pt films have small grain size (about 400 nm), as shown in figure 8, and this high density of grain-boundary affects the high resistivity of the films.

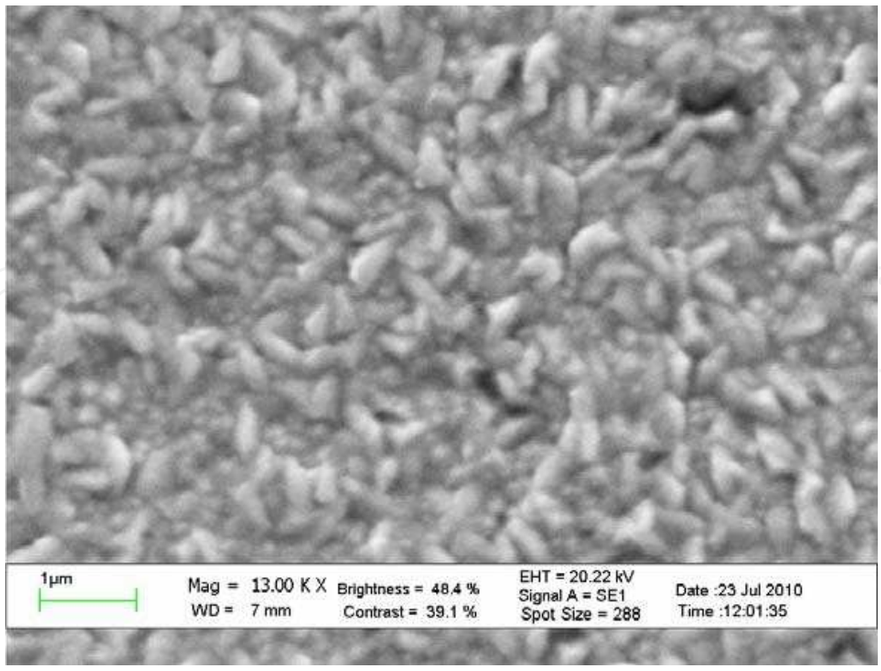

Fig. 8. SEM photo of the as deposited Pt film

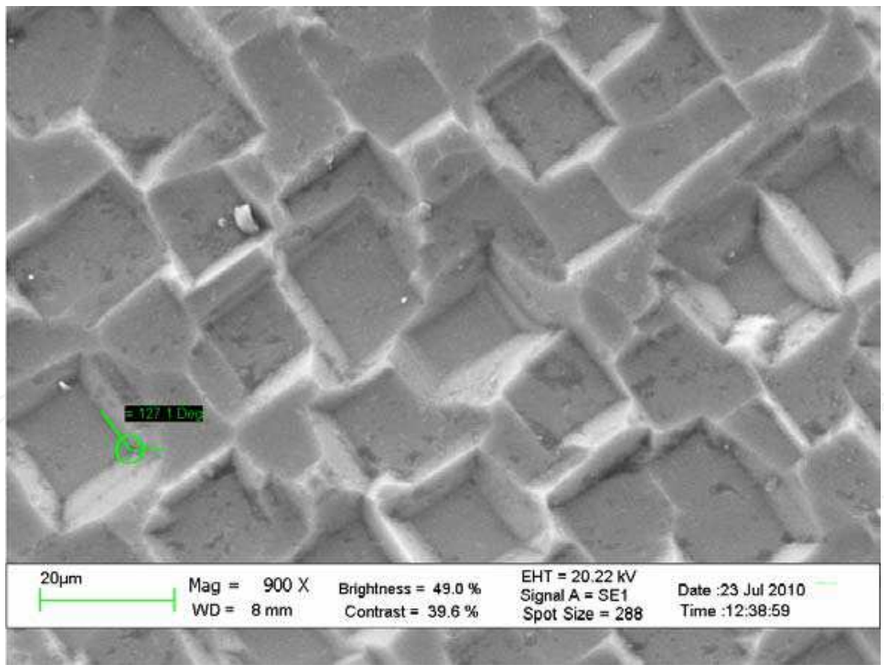

Fig. 9. SEM photo of the 32 hours annealed Pt film

Moreover, the as-grown films contain a number of structural defects that anneal out when heat treatment is carried out and, as a result, the film's resistivity decreases. The Pt annealing results in the relaxation of intrinsic stresses, as well as in the redistribution of structural imperfections: grains coalescence take place and the film sheet resistivity

decreases. SEM photo of the 32 hours annealed sample, shown in figure 9, demonstrates that recrystallization of Pt surface occurs [14].
The unannealed outer Pt film was silvery while the annealed films were matt: this color change can be explained with the increase of the Pt grain size. The adhesion strength of the Pt films was good enough to pass a rudimentary "tape test" with a transparent tape after each anneal as well.

3.2 c-AlN/(0001)-Al_2O_3

Highly c-axis oriented AlN films were grown by rf reactive sputtering technique on the polished surface of (0001) oriented single crystal Al_2O_3 substrate. Then the as grown films, 0.26 to 4.7 μm thick, were thermally annealed at 900°C in air for 1 to 18 hours and the AlN structural characteristics were evaluated after each thermal cycle. References are available in the literature concerning the high thermal annealing (HTA) of AlN on Si performed at 700 – 1200 °C for 2 to 12 hours in controlled atmosphere (in oxygen or nitrogen flux) or in high vacuum; AlN films on Al_2O_3 were heated at 950 °C in air for 30 minutes [20] to 1 hour [21], at 900 to 1200 °C for 10 s in flowing N_2[22], and at 800 °C for 90 minutes in air [23]; bulk AlN was annealed in oxygen at 900 – 1150 °C for 6 hours [24]. In the present work, the HTA of the AlN films on Si and on Al_2O_3 substrates have been performed up to 32 and 18 hours, respectively. No damage was observed on the surface of the AlN/Al_2O_3 film even after 18 hours annealing: the AlN films were still clear, uniform, and extremely adhesive to the substrate. The impact of the annealing on the films structural properties was investigated by XRD before and after undergoing the thermal annealing. The D and *c* parameter of the AlN films thermally annealed for different time periods, are listed in tab. 1.

AlN thickness (μm)	Time (hours)	$FWHM_{\theta-2\theta}$ (deg)	D (Å)	c (Å)
4.7	0	0.384	218	4.995
	4	0.281	297	4.977
	8	0.289	288	4.978
	12	0.290	290	4.978
4	0	0.270	540	4.976
	1	0.269	548	5.024
	3	0.264	555	5.026
	5	0.262	593	5.027
	9	0.261	611	5.037
	18	-	-	-
1.5	0	0.289	252	4.978
	4	0.332	288	4.984
	8	0.350	281	4.989
	10	0.410	303	5.001
0.26	0	0.500	220	4.986
	3	0.422	198	5.048
	4	-	-	-

Table 1. The AlN (002) FWHM, the D and *c* parameter of the AlN films thermally annealed for different time periods

Figures 10, 11 and 12 show the diffraction patterns of the AlN films, 4.0, 1.5 and 4.7 μm thick, annealed for different time.

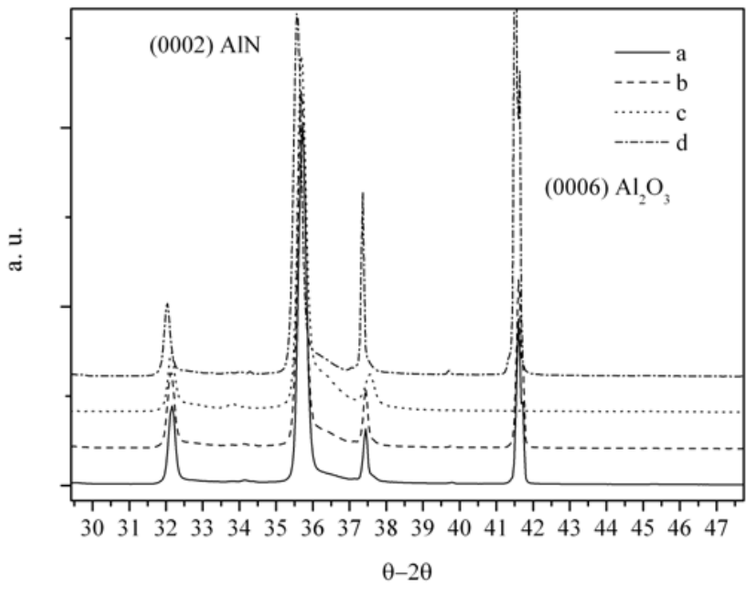

Fig. 10. XRD pattern of the AlN, 4 μm thick, annealed for 1 (a), 3 (b), 5 (c), and 9 (d) hours

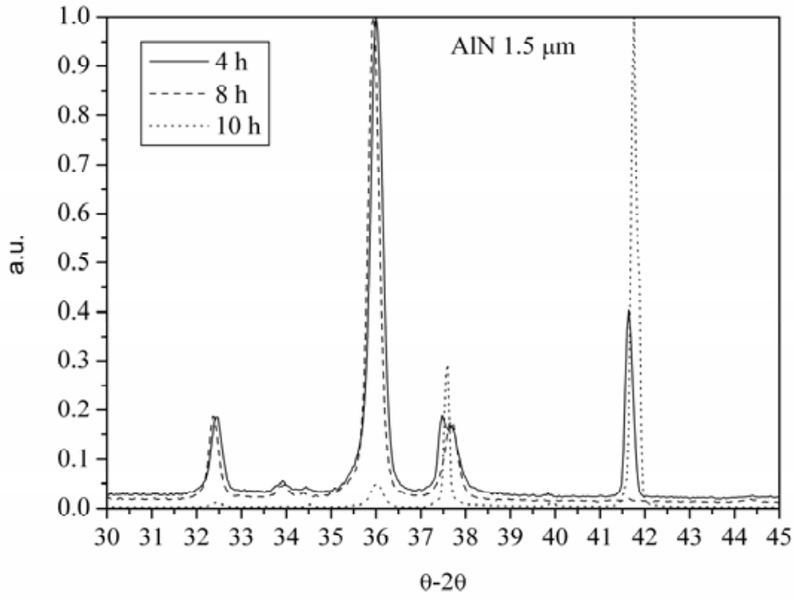

Fig. 11. XRD pattern of the AlN, 1.5 μm thick, annealed for 4, 8 and 10 hours

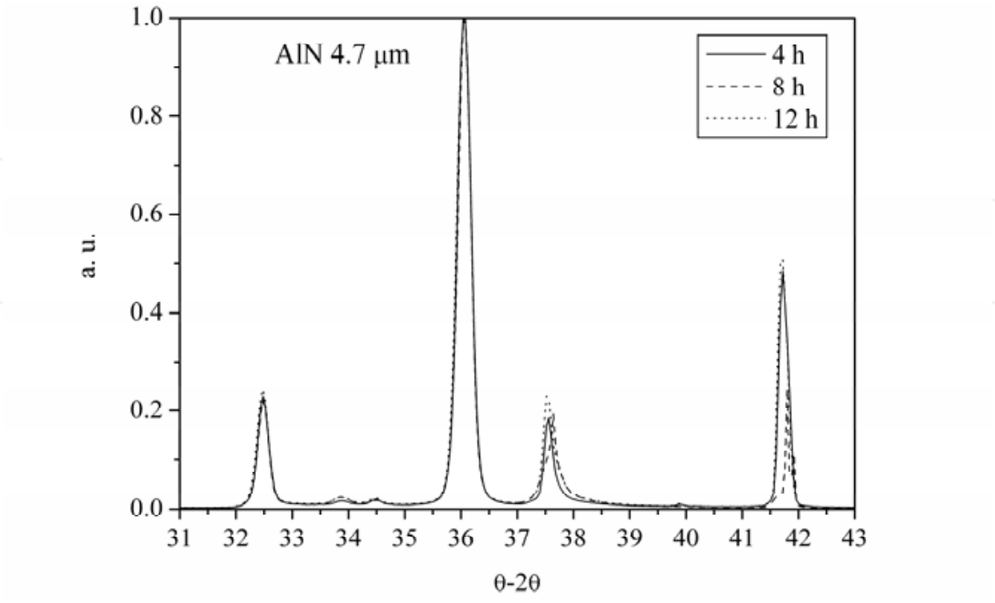

Fig. 12. XRD pattern of the AlN, 4.7 μm thick, annealed for 4, 8 and 12 hours

The AlN (0002) peak at approximately 2θ = 36° of the as deposited films, 0.26 to 4.7 μm thick, showed a FWHM (from θ-2θ scan) in the range 0.5° to 0.27°. Both the as grown and the annealed samples exhibit a strong peak at 2θ ~ 42° due to the (0006) reflection of the Al_2O_3 substrate, and one small peak at 76°, corresponding to the (0004) reflections of the wurtzite AlN structure, not shown in figures 10 to 12. The 2nd order peaks of AlN(0002) and Al_2O_3 (00001) are clearly visible at ~32.4° and ~37.5°. After 4 hours at 900°C in air, the (0002) peak of the thin AlN film (0.26 μm thick) broadens completely as well as that of the 4 μm thick AlN film after 18 hours annealing. No other AlN phases are present, nor AlN-oxide traces are evident in the spectra after the annealing; only a decrease in the 2θ value of the (0002) peak is observed, resulting in an increase in the c lattice parameter whose values are larger than the bulk lattice parameter [13], indicating the presence of compressive stress in the surface plane. This lattice elongation, perpendicular to the growth plane, is usually associated with the intrinsic compressive stress caused by the lattice mismatch between the AlN and Al_2O_3, $(a_{sapphire}-a_{AlN})/a_{sapphire}$, that is approximately equal to 30%. Our previous results [25] have shown that the *c*-axis of the as grown AlN films on sapphire relaxes to the bulk value with increasing the film thickness: an interface layer, strained because of the large lattice mismatch, is formed on the sapphire surface and is followed by a columnar AlN layer which runs through the entire thickness of the film. The thinner the AlN film and more is strained and unable to survive to the HTA.

4. Conclusions

Highly c-axis oriented AlN films and thin film stacks of Pt/AlN/Pt were sputtered at 180°C on (0001)Al_2O_3 substrates and at 200°C on oxidized Si substrates. The multilayers were heated at 900 °C in air up to 32 hours to test their resistance to high temperature. The

structural investigation of the annealed films showed that the thermal annealing improved the crystal quality of the AlN films sandwiched between the Pt films, as confirmed by the decreased FWHM of the rocking curves, and the film piezoelectric d_{33f} coefficient resulted unaffected by the temperature. The study of the electrical, morphological and structural characteristics of the Pt electrode revealed a dense surface with a hillock-free morphology, confirming that Pt is the material of choice when a high oxidation resistance is required for metallic components within devices operating at elevated temperatures. The AlN films on sapphire show a lattice elongation, perpendicular to the growth plane, that is usually associated with the compressive stress caused in the growth plane by the lattice mismatch between the film and the substrate. After the first few hours annealing, the FWHM of the (002) AlN peak decreases showing an improvement in the film texture; further annealing results in the FWHM broadening, whose magnitude depends on the film thickness. The structural investigations of thin (0.26 μm) and thick (from 2 to 4.7 μm) annealed AlN films revealed that the film behaviour in harsh environment is strongly affected by the film properties. Thick films, whose structure is more relaxed than the thin one, is able to survive to high temperature without suffering significant deterioration for longer annealing times than the thin one. The obtained results confirm that, during the HTA, the Pt film on the substrate surface is protected by the AlN film, while the Pt film directly exposed to the ambient conditions acts as a protective layer with respect to the AlN film; thus the AlN-based STFM coupling configuration to be implemented on sapphire or silicon substrates is an attractive alternative to langasite and $GaPO_4$ for the development of microwave electroacoustic devices able to work at high temperatures.

5. Acknowledgements

The author wishes to thank Mr. P.M. Latino for his technical support in the development of the technological processes and the HTA.

6. References

[1] Hauser, R. Reindl, L. Biniasch, J., ú *Ultrasonics Symposium*, Vol. 1, 192 (2003).
[2] M. Pereira da Cunha, M.P. Saulo de A. Fagundes, ú *Ultrasonics Symposium*, Vol. 1, 283 (1998).
[3] Maurício Pereira da Cunha, Eric L. Adler and Donald C. Malocha, ú *Ultrasonics Symposium*, Vol.1 169 (1999).
[4] Kar, J.P., Mukherjee, S., Bose, G., Tuli, S., Myoung, J.M., *Materials Science and Technology*, 25 1023 (2009).
[5] Zhigang Lin and Yoon, R.J., International Symposium on *Advanced Packaging Materials: Processes, Properties and Interfaces*, 156 (2005).
[6] C. Zolper, D. J. Rieger, and A. G. Baca S. J. Pearton and J. W. Lee R. A. Stall, *Appl. Phys. Lett.* 69, 538 (1996).
[7] S.M.Middelhoek, S.A.Audet, *Silicon sensors*, Academic Press, London 1989.
[8] M.J.Vellekoop, E.Nieuwkoop, J.C.Hsaartsen, A.Venema, ú *Ultrasonics Symposium*,Vol. 1, 375 (1981).
[9] E.L. Adler, G.W. Farnell, J. Slaboszewicz, C.K. Jen, ú *Ultrasonics Symposium,* Vol. 1, 103 (1982).
[10] K. Tsubouchi, K. Sugai, N. Mikoshiba, ú *Ultrasonics Symposium,* Vol. 1, 375 (1981).

[11] J.G. Gualtieri, J.A. Kosinski, A.Ballato, ú *Ultrasonics Symposium,* Vol. 1 403 (1992).
[12] C. Caliendo, *Appl. Phys. Letters* 92 103501 (2008).
[13] JPCDS cards No. 25-1133 Powder Diffraction File, Joint Committee on Powder Diffraction Standards, ASTM, Philadelphia, PA, 1967, Card 25-1133
[14] C. Caliendo, P. M. Latino, *Thin Solid Films* 519 (2011), pp. 6326-6329
[15] C.K.Xu, V.N.Umashev, I.B.Yakovkin, *Sov. Phys*. PTE6, 192 (1986).
[16] Landolt-Bornstein, *Numerical Data and Functional Relationships in Science and Technology, Group III: Crystal and Solid State Physics*, (Springer-Verlag Berlin, Heidelberg-New York, 1979), Vol. 11 (1979).
[17] C.-Y. Lin, F.-H. Lu, *J. Eur. Ceram. Soc*. 28 691 (2008).
[18] E. A. Chowdhury, J. Kolodzey, J. O. Olowolafe, G. Qiu, G. Katulka, D. Hits, M. Dashiell, D. van der Weide, C. P. Swann, K. M. Unruhm, *Appl. Phys. Lett*. 70 2732 (1997).
[19] F. Jose, R Ramaseshan, S. Dash, S. Bera, A. K. Tyagi, B. Raj, *J. Phys. D: Appl. Phys*. 43 075304 (2010).
[20] T. Aubert, O. Elmazria, B. Assouar, L. Bouvot, M. Oudich, *Appl. Phys. Lett*. 96 2035031 (2010).
[21] S.-K. Tien, C.-H. Lin, Y.-Z. Tsai and J.-G. Duh, *J. Alloys Compd*. 489 237 (2010).
[22] Z. Gu, J.H. Edgar, S.A. Spekman, D. Blom, J. Perrin, J. Chaudhuri, *J. Electron. Mater*. 34 1271 (2005).
[23] T. Aubert, M. B. Assouar, O. Legrani, O. Elmazria, C. Tiusan, S. Robert, *J. Vac. Sci. Technol. A* 29 021010 (2011).
[24] B. Liu, J. Gao, K.M. Wu, C. Liu, *Solid State Commun*. 149 715 (2009).
[25] C. Caliendo, P. Imperatori, *J. Appl. Phys.* 96, 2610 (2004).

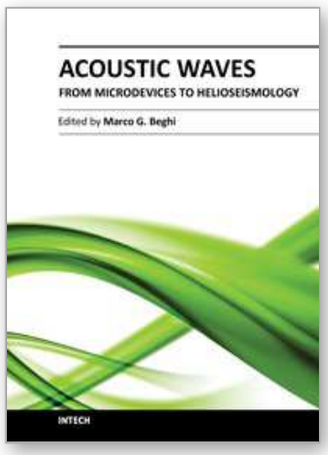

Acoustic Waves - From Microdevices to Helioseismology

Edited by Prof. Marco G. Beghi

ISBN 978-953-307-572-3
Hard cover, 652 pages
Publisher InTech
Published online 14, November, 2011
Published in print edition November, 2011

The concept of acoustic wave is a pervasive one, which emerges in any type of medium, from solids to plasmas, at length and time scales ranging from sub-micrometric layers in microdevices to seismic waves in the Sun's interior. This book presents several aspects of the active research ongoing in this field. Theoretical efforts are leading to a deeper understanding of phenomena, also in complicated environments like the solar surface boundary. Acoustic waves are a flexible probe to investigate the properties of very different systems, from thin inorganic layers to ripening cheese to biological systems. Acoustic waves are also a tool to manipulate matter, from the delicate evaporation of biomolecules to be analysed, to the phase transitions induced by intense shock waves. And a whole class of widespread microdevices, including filters and sensors, is based on the behaviour of acoustic waves propagating in thin layers. The search for better performances is driving to new materials for these devices, and to more refined tools for their analysis.

InTech Europe
University Campus STeP Ri
Slavka Krautzeka 83/A
51000 Rijeka, Croatia
Phone: +385 (51) 770 447
Fax: +385 (51) 686 166
www.intechopen.com

InTech China
Unit 405, Office Block, Hotel Equatorial Shanghai
No.65, Yan An Road (West), Shanghai, 200040, China
中国上海市延安西路65号上海国际贵都大饭店办公楼405单元
Phone: +86-21-62489820
Fax: +86-21-62489821

IntechOpen